Eur Radiol (2011) 21:1397–1405
DOI 10.1007/s00330-011-2074-x

CHEST

MRI assessment of thoracic stent grafts after emergency implantation in multi trauma patients: a feasibility study

Volker Rasche · Alexander Oberhuber · Stephan Trumpp · Axel Bornstedt · Karl-Heinz Orend · Nico Merkle · Wolfgang Rottbauer · Martin Hoffmann

Received: 4 October 2010 / Revised: 13 December 2010 / Accepted: 15 December 2010 / Published online: 18 February 2011
© European Society of Radiology 2011

Abstract
Purpose To evaluate the feasibility of MRI for static and dynamic assessment of the deployment of thoracic aortic stent grafts after emergency implantation in trauma patients.
Methods Twenty patients initially presenting with a rupture of the thoracic aorta were enrolled in this study. All patients underwent thoracic endovascular aortic repair (TEVAR). The deployment of the implanted stent graft was assessed by CTA and MRI, comprising the assessment of the aortic arch with and without contrast agent, and the assessment of the motion of the stent graft over the cardiac cycle.
Results The stent graft geometry and motion over the cardiac cycle were assessable by MRI in all patients. Flow-mediated signal variations in areas of flow acceleration could be well visualised. No statistically significant differences in stent-graft diameters were observed between CT and MRI measurements.
Conclusion MRI appears to be a valuable tool for the assessment of thoracic stent grafts. It shows similar performance in the accurate assessment of stent-graft dimensions to the current gold standard CTA. Its capability of providing additional functional information and the lack of ionising radiation and nephrotoxic contrast agents may make MRI a valuable tool for monitoring patients after TEVAR.

Keywords Thoracic endovascular aortic repair · Magnetic resonance imaging · Computer tomography · Cine imaging

V. Rasche · S. Trumpp · A. Bornstedt · N. Merkle · W. Rottbauer
Department of Internal Medicine II, University Hospital Ulm,
Albert-Einstein-Allee 23,
89081 Ulm, Germany

A. Oberhuber · S. Trumpp · K.-H. Orend
Department of Vascular and Thoracic Surgery,
University Hospital Ulm,
Steinhövelstr. 9,
89075 Ulm, Germany

M. Hoffmann
Department of Diagnostic and Interventional Radiology,
University Hospital Ulm,
Steinhövelstr. 9,
89075 Ulm, Germany

V. Rasche (✉)
Department of Internal Medicine II, University Hospital Ulm,
University of Ulm,
Robert-Koch-Str.8,
89081 Ulm, Germany
e-mail: volker.rasche@uniklinik-ulm.de

Introduction

Thoracic Endovascular Aortic Repair (TEVAR) of various aortic abnormalities has turned out to be an attractive alternative option to conventional surgical approaches [1–6]. Contrary to conventional open surgery, however, TEVAR may be associated with graft-related complications such as endoleaks, kinking, infolding or even stent-graft migration. Stent-graft disconformability and disattachment phenomena at the inner aortic arch radius in juvenile trauma victims have been identified as a relevant issue [7, 8]. Therefore lifelong regular follow-up by tomographic imaging is required for close monitoring of all patients treated with thoracic aortic stent grafts.

Multislice volumetric CT still represents the imaging gold standard for the assessment of the stent graft. However, its related X-ray dose and the nephrotoxicity of the required contrast agent limits its frequent application, especially in younger patients and in patients with renal insufficiency. Standard CTA is performed without ECG-

registration and, hence, it does not provide any data on the stent graft's dynamics over the cardiac cycle and its impact on the haemodynamic flow patterns.

Over the last decade, magnetic resonance angiography (MRA) has been incorporated into diagnostic routine for the assessment of aortic abnormalities, currently challenging CTA and X-ray angiography as the imaging methods of choice [9]. The versatility of MRI enables a variety of imaging protocols comprising contrast agent-enhanced [10] and unenhanced angiography [11, 12], black-blood techniques for vessel wall assessment [13], and especially the ability to visualise and quantify functional parameters such as vessel wall compliance [14] and blood flow [15, 16]. The application of MRI in patients with endovascular stent grafts is not commonly performed. The image quality is often compromised by susceptibility artefacts introduced by the stent material [17] or severe signal reduction in the stent graft due to RF shielding of the mesh [18]. Furthermore, safety issues such as RF heating and dislocation must be carefully considered [19]. However, with the increasing awareness of the importance of MRI in general, stent grafts are increasingly manufactured with MR-compatible materials and safety issues as well as image quality issues should become of minor importance [20–23]. In direct comparison to CT, MRI has proven to provide all relevant information required for follow-up of endoluminally treated abdominal aortic aneurysm [23–27] with superior performance in the assessment of thrombus reorganisation [27] and inferior performance in the identification of stent fracture [23].

The objective of this work was to prove the feasibility of MRI as a comprehensive imaging tool for the assessment of thoracic stent grafts, including disattachment phenomena, its dynamics over the cardiac cycle and its impact on haemodynamics.

Materials and methods

Patients

Twenty consecutive trauma patients (7 female, 13 male; mean age 36±15; 8–2417d after intervention) were enrolled in this feasibility study. All patients initially presented with aortic rupture at the transition zone of the arch and descending segment of the thoracic aorta. The rupture site was treated with endovascular stent graft procedures in all patients. In 11 patients, a Medtronic Valiant stent graft (MRI safe up to 3 T) and in 9 patients a Gore excluder TAG stent graft (MRI safe up to 1.5 T) were implanted.

The study protocol was approved by the local ethics committee and informed written consent was obtained from all patients at least 24 h before the MRI investigation.

Imaging protocols

All patients underwent conventional contrast agent (CA)-enhanced routine CTA followed by the investigational comprehensive MRI protocol.

The CTAs were conducted on a 64-slice clinical CT system (Brilliance 64, Philips Medical Systems, The Netherlands). Imaging was performed after injection of 90 ml CA at an injection rate of 4.5 ml/s and at a spatial resolution of $0.6\times0.6\times0.9$ mm^3.

Magnetic resonance imaging acquisitions were performed on a 1.5 T Philips Gyroscan Intera system (Philips Medical Systems, Best, The Netherlands), equipped with a PowerTrak6000 gradient system (23mT/m; 219 μs rise time). All data were acquired using a dedicated cardiac 5- or 32-element phased array coil and a vector electrocardiogram (ECG) module was applied for ECG triggering and recording.

The MRI protocol comprised:

- Preparation imaging
  For localisation, three orthogonal stacks in transversal, sagittal and coronal slice orientation were acquired applying a multi-slice segmented steady-state free precession (SSFP) gradient echo technique. Acquisition was performed in a single breath-hold with a typical acquisition time of 15 s. Subsequently, the coil sensitivity profiles were measured as a prerequisite for subsequent parallel imaging protocols and for compensation of coil sensitivity-induced intensity variations in the images.
- MR Aortic angiography
  MR Angiograms of the aorta were acquired in parasagittal geometry covering the left ventricular outflow tract, the ascending aorta, the aortic arch and the thoracic descending aorta. Acquisitions comprise a three-dimensional SSFP sequence (Angio) followed by a contrast agent (Magnevist©, Schering, Germany)-enhanced three-dimensional T1-weighted fast gradient echo acquisition (CE-Angio). Imaging was performed after injection of a CA bolus of 30 ml CA at an injection rate of 4 ml/s. Bolus timing was determined by monitoring the intensity in the thoracic aorta after injection of a test bolus (2 ml, 4 ml/s).
- Cardiac phase resolved MR imaging
  Dynamic assessment of the stent graft over the cardiac cycle was visualised applying a cardiac phase resolved, retrospectively ECG-gated SSFP multi-slice acquisition technique (CINE), providing 40 heart phases. Respiratory motion was controlled by multiple breath-holds ensuring a maximal breath-hold length of 10 s. Three stacks of 9 slices each were acquired centred at the proximal end, the centre and

Table 1 MR acquisition parameters

	Angio	CE-Angio	Cine
FOV [mm]	300×300×150	400×360×84	380×347×6
Resolution [mm]	1.8×1.8×1.5	1.0×1.7×4.0	1.2×1.2×6.0
TE [ms]	1.9	1.3	1.7
TR [ms]	3.8	4.9	3.4
Flip angle [°]	90	40	60
Turbo factor	39	NA	14
Cardiac phases	1	1	40
Acq. Duration [ms]	149	NA	23
Imaging duration [s]	217	21	11

FOV field of view, *TE* echo time, *TR* repetition time, *CE* contrast-enhanced

the distal end of the stent graft. All stacks were aligned perpendicular to the centreline of the stent graft.

Details of the MR acquisition protocols are provided in Table 1.

Data evaluation

All patient data were reviewed by two experienced readers.

The general image quality was ranked regarding the appreciation of the stent graft geometry Q_G, dynamics Q_D, and visibility of flow-mediated Q_F artefacts on a 1 (poor) to 5 (excellent) scale. Qualitative assessment of the stent-graft motion Q_M over the cardiac cycle was ranked on a 1 (no apparent motion) to 3 (strong apparent motion) scale, independently for the proximal and distal segments of the stent. The deployment of the stent Q_d against the vessel wall was qualitatively assessed on a 1 (attached to the vessel wall) to 3 (large areas of the stent not attached to the vessel wall) scale.

The stent-graft diameters were quantified at three levels within the stent graft. Before quantification, the MRI and CT data were registered applying a mutual information rigid-body registration (Slicer V3.6, http://www.slicer.org, [28–30]). Diameter measurements were done at similar positions in the registered data sets by manual identification of opposite stent struts. On CT, the strut position was identified as the centre of the bright metal signal and on the MRI the centre of the respective signal void.

Statistical analysis

Continuous variables are given as mean±standard deviation (SD). Bland-Altman analysis, given in mean differences (MD)±SD, was performed to assess inter-observer and inter-technique variability. Statistical significance of the continuous variables was tested by a two-tailed paired Student's *t*-test. The statistical significance of the differences in stent motion was assessed applying a Wilcoxon signed rank test. P values below 0.05 were considered significant.

Results

The MRI imaging protocol could be completed in all patients. The average acquisition time for the entire MRI examination was 32±10 min.

A direct comparison of the appearance of the stent graft between native and contrast-enhanced MRI is provided in Fig. 1. As expected, the artefacts introduced by the stent grafts appear more pronounced on the native SSFP images compared with the contrast-enhanced acquisitions obtained with the T1-weighted fast gradient echo technique. The artefacts introduced by the stent facilitate its delineation. The SSFP images appear superior in the assessment of the deployment of the stent. However, on the native images, a

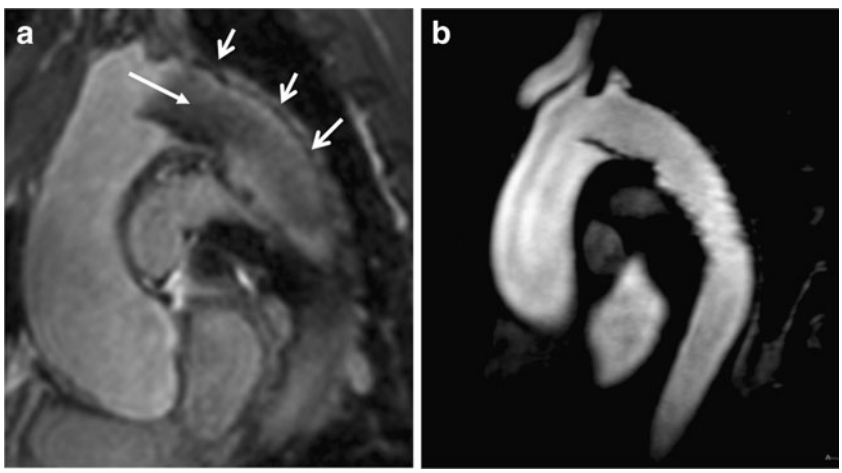

Fig. 1 Non-contrast (**a**) and contrast agent-enhanced (**b**) MRI. The delineation of the stent graft (*open arrow heads*) appears better in (**a**), while the signal homogeneity in the aorta (*closed arrow head*) appears superior in (**b**)

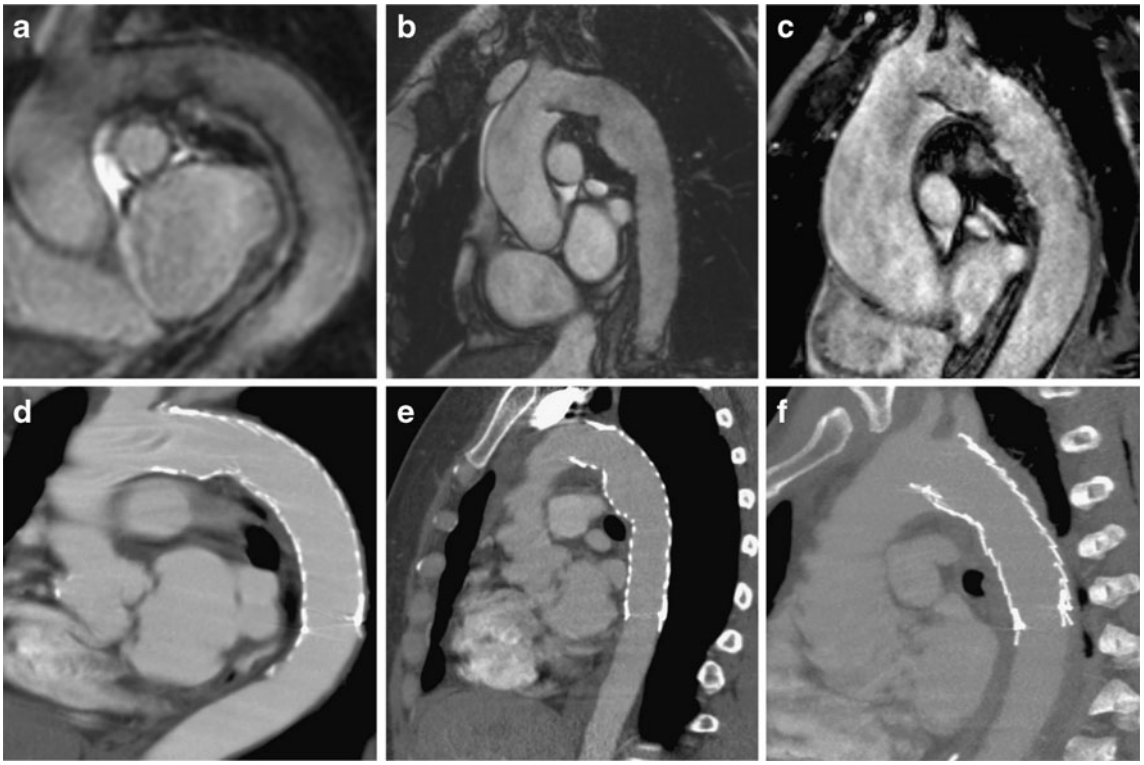

Fig. 2 Non-contrast agent-enhanced MRI (**a**–**c**) and respective CTA (**d**–**f**) visualisation of thoracic stent grafts. Because of the different contrast mechanism, contrary to CTA the stent struts appear black on MRI

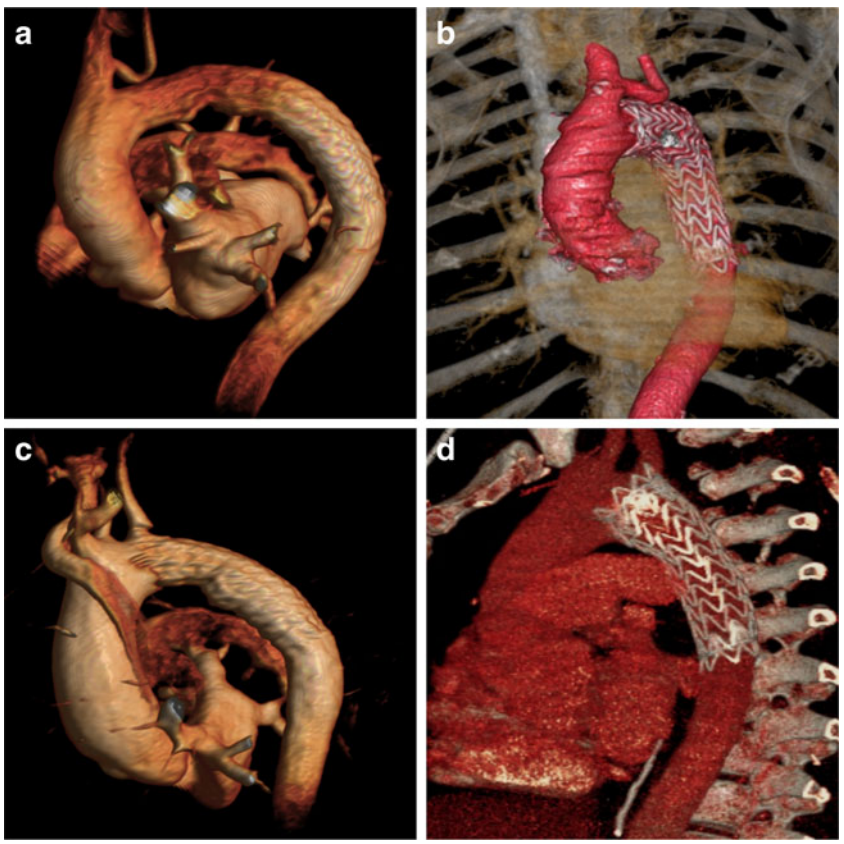

Fig. 3 Volume visualisation of the stented thoracic artery by contrast-enhanced MRA (**a**, **c**) in comparison to CTA (**b**, **d**). As the stent is not directly visible on MRA, its location in the thoracic aorta can only indirectly be assessed according to the irregular shape of the surface

more pronounced intensity drop can be appreciated within the stent, likely caused by RF shielding effects, which are less obvious on the contrast-enhanced acquisitions.

In all patients, the geometry of the stent graft could be obtained with at least mediocre image quality (mean ranking Q_G=4.2 ± 0.75), allowing the assessment of the deployment of the stent against the vessel wall. In direct comparison to CT (Fig. 2), no obvious loss of morphological information of the stented thoracic aorta was observed. Because of the inferior spatial resolution and resulting signal voids close to the stent struts on MRA, the delineation of the stent struts appears superior on CTA. Owing to the gated acquisition, however, motion blur and motion-induced artefacts, especially in the ascending aorta, can be avoided by MRA. Furthermore, long-range metal artefacts introduced by the stent can be almost completely suppressed. On CTA as well as on MRA similar results regarding the assessment of the disattachment of the stents were observed. In only two patients was a perfect deployment of the stent achieved (Fig. 2a,d), in most of the patients (n=11) some minor (Fig. 2b,e) and in seven patients a large section of the stent graft (Fig. 2c, f) was not properly attached to the vessel wall due to the narrow aortic arch geometry.

In all CA-enhanced MRA data, sufficient image quality could be obtained for volume visualisation of the aorta as shown in Fig. 3. In comparison to CTA (Fig. 3b,d), it becomes obvious that due to the different contrast mechanism, in MRA (Fig. 3a,c), the stent struts cannot be visualised directly. Nonetheless, the volume visualisation appears sufficient for a quick overview of the morphology of the aorta after stent graft implantation. The location of the stent graft can be appreciated by the irregularly shaped surface in that region.

The dynamics of the stent were assessable in all patients (mean ranking Q_D=3.7±0.76). Although the image quality during systole suffered from superimposed flow artefacts in seven cases, the motion of the stent could be nicely appreciated over the entire cardiac cycle in all data sets. Stent motion was significantly ($p<0.001$) more pronounced in the proximal section (no motion n=2; moderate motion n =13, strong motion n=5) compared with the distal section (no motion n=18; moderate motion n=2, strong motion n=0). Observed graft motion over the cardiac cycle is exemplarily depicted in Fig. 4 for a proximal and in Fig. 5 for a distal segment of the stent graft. Side-by-side comparison of the end-diastolic and the end-systolic location of the stent graft relative to the vessel wall reveals a variation of the stent position in its proximal section to the order of 5 mm with a related change in the angle between the stent and the vessel wall of 21°. In the distal example, a

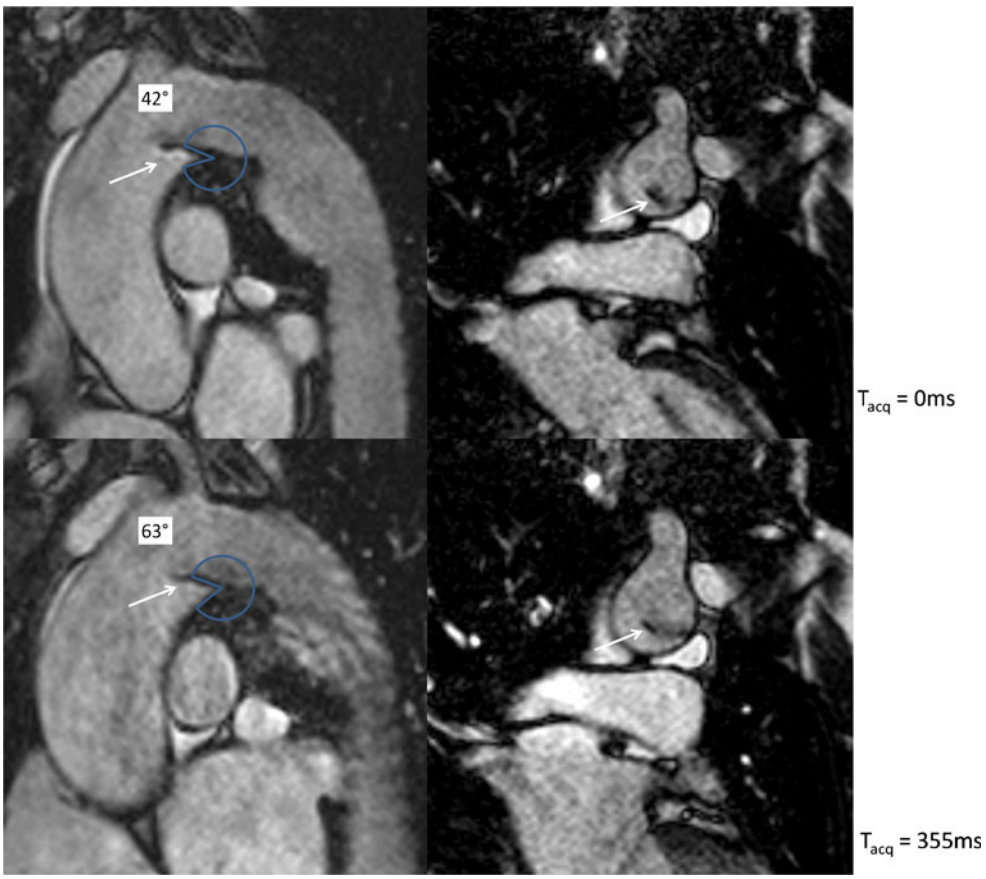

Fig. 4 Comparison of the location of the stent graft (*arrows*) during end-diastole (*top*) and end-systole (*bottom*) reveals a dislocation of the stent of several mm in the parasagittal (*left*) as well as in the orthogonal (*right*) view

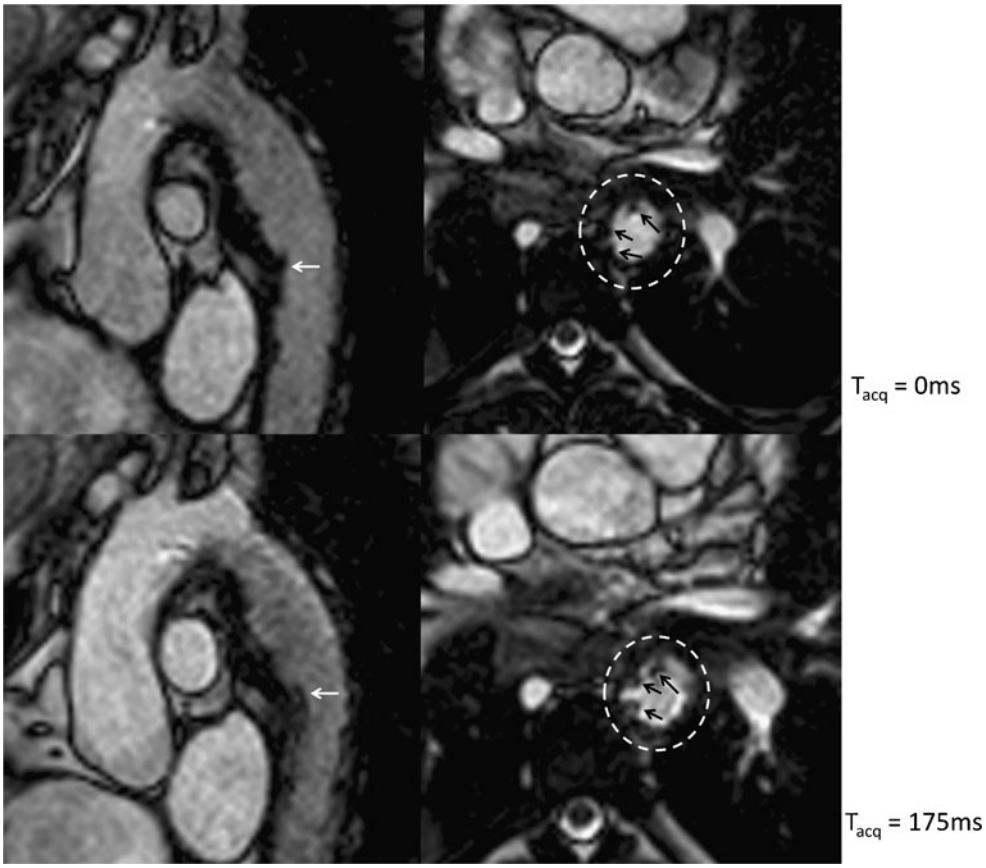

Fig. 5 Comparison of the location of the stent graft (*arrows*) during end-diastole (*top*) and end-systole (*bottom*) reveals a separation of the stent from the vessel wall over the cardiac cycle

clear separation of the stent from the vessel wall during systole can be appreciated.

Qualitative assessment of flow-induced artefacts was possible in all patients (mean ranking Q_F=3.5±0.93). In the event of slightly obstructing stent grafts, a clear flow-mediated signal void could be observed (Fig. 6) indicating significant flow acceleration.

Excellent agreement (R^2=0.94) between the MRI- and CT-derived measurements of the stent-graft diameter was observed (Fig. 7). The resulting mean differences were −0.23±1 mm (p=0.1) for reviewer 1 and −0.1±1.1 mm (p=0.45) for reviewer 2. Although the differences were not statistically significant, a slight trend towards overestimation of the diameter by MRI was observed. The intra-observer variability was −0.14±1 mm (p=0.3) for MRI and 0±0.9 mm (p=0.85) for CT. The respective Bland-Altman plots are provided in Fig. 8.

Discussion

As demonstrated, the application of MRI for the assessment of endovascular thoracic aorta repair by means of stent

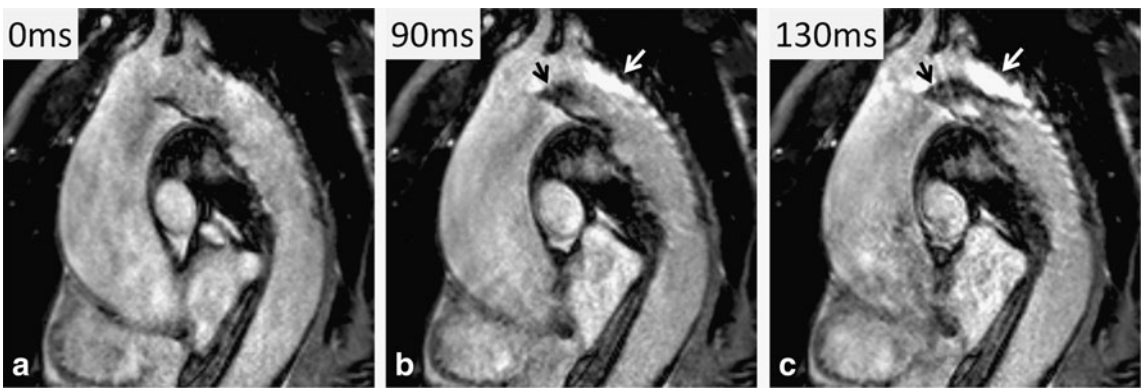

Fig. 6 Qualitative visualisation of the flow-mediated image artefacts (*arrows*) during end-diastole (**a**) and during systole (**b**, **c**). Times are given relative to the preceding R-peak of the ECG

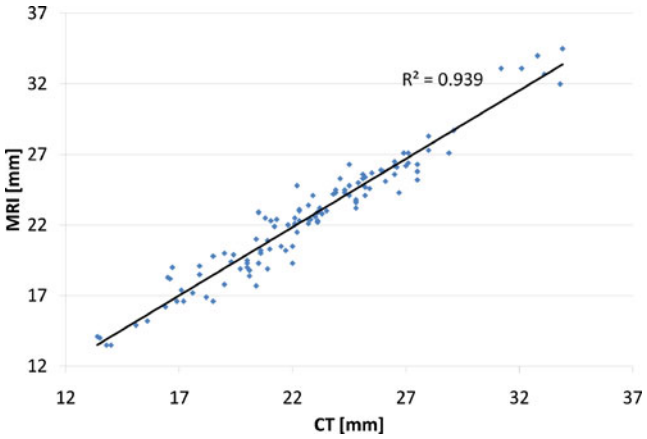

Fig. 7 Scatter plot of the diameters obtained by CT (*horizontal axis*) and MR (*vertical axis*)

grafts appears feasible. In direct comparison to the current gold standard CT, the attractiveness of MRI results from its capability of providing functional information of the dynamics of the stent and to visualise the impact of the stent on haemodynamics. Further advantages include the complete avoidance of nephrotoxic contrast agents and ionising radiation.

MRI contrast agents are known to be safe and only minor adverse effects such as nausea, taste perversion, and hives have been infrequently reported. However, in 2006 several groups reported a strong association of the development of nephrogenic system fibrosis (NSF) and the administration of Gd3+-based contrast agents [31, 32] in a subset of patients with advanced renal disease. However, current evidence suggests that the risk of developing NSF is related to the physiochemical properties of the chelate complex and no case of NFS has been reported for cyclic structured compounds so far. Thus the risk of developing NFS even during long-term annual monitoring can likely be avoided by choosing an adequate chelate complex.

Possible limitations in MRI may arise from MR-incompatible stent grafts or other implanted devices, which may cause severe image artefacts or even complete signal voids on the resulting images. Furthermore, ferromagnetic or elongated implants/devices are prone to cause a major risk for the patient due to resulting mechanical forces or implant/device heating. However, most recent implants/devices are MR-safe up to a field strength of at least 1.5 T. Although most trauma patients in our study had multiple implants for bone fracture fixation, none of the patients had to be excluded for safety reasons or because of impaired image quality.

In the investigated patient cohort, all imaging could be completed successfully, with at least mediocre image quality for static as well as functional MRI acquisitions, indicating a good applicability of MRI even in multi-traumatic patients. The tendency of MRI to overestimate

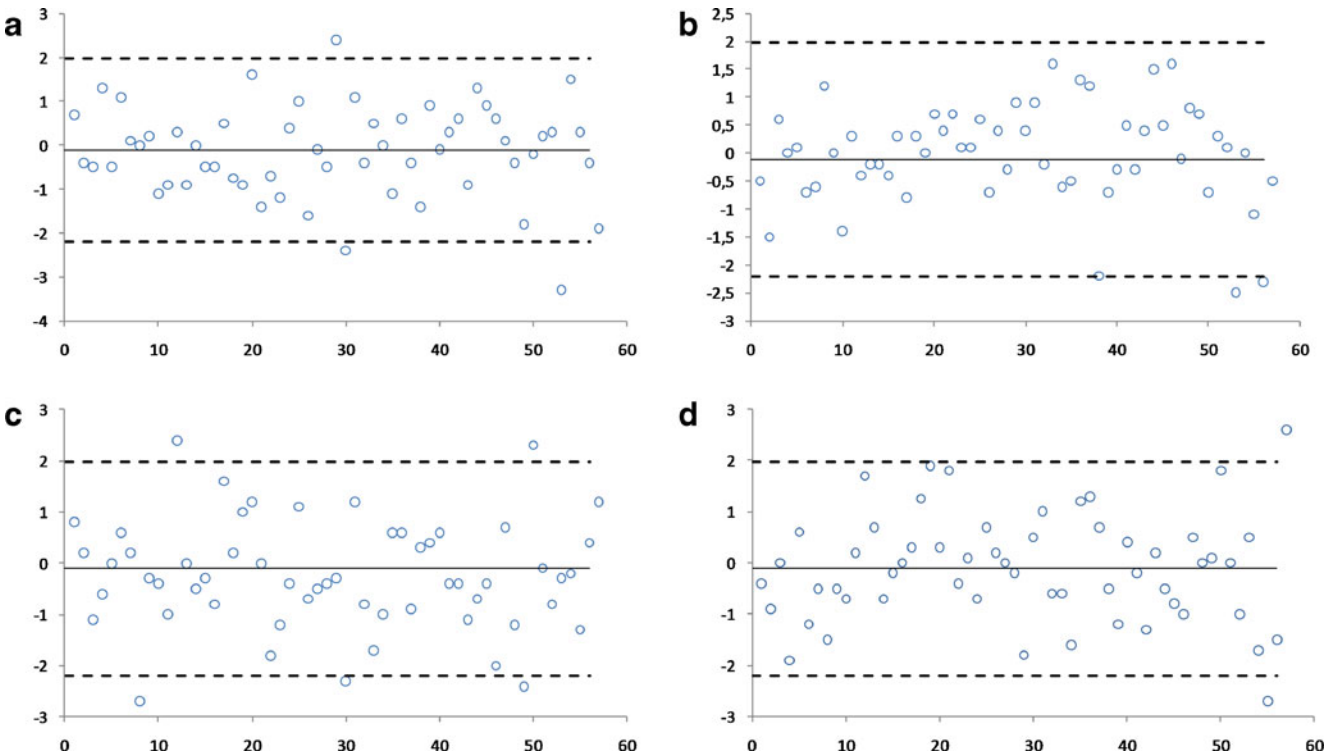

Fig. 8 Bland-Altman plots of the intra-observer variability for MRI (**a**) and CT (**b**), and the intra-technique variability for reviewer 1 (**c**) and reviewer 2 (**d**)

stent diameters can be explained by its inferior spatial resolution and the often blurred appearance of the stent struts. However, the observed differences are well below the previously published reproducibility of diameter quantification [33, 34] with CTA.

In general, motion of the stent was much more pronounced in the proximal section compared with the distal segments. In those patients showing significant narrowing of the aortic arch due to free floating proximal segments of the stent graft, a significant flow-induced mediation of the blood signal could be observed, often with a cardiac phase-dependent movement of the stent relative to the vessel wall. In two patients, separation of the distal section of the stent graft from the descending aortic vessel wall was observed. The impact of the observed stent graft motion on the long-term patient outcome is still to be evaluated in further studies.

Limitations of the current study include the absence of data for long-term follow-up and the lack of patients with complications. Furthermore, it is restricted to trauma patients all initially presenting with aortic rupture at the transition zone of the arch and descending segment of the thoracic aorta. Thus, from the current data, the performance of MRI as general imaging tool for the identification of TEVAR related complications and long-term follow-up cannot yet be concluded.

In conclusion, MRI can provide a comprehensive assessment of thoracic aortic stent grafts after percutaneous implantation. The feasibility of assessing the stent graft geometry as well as motion without any need for ionising radiation or nephrotoxic contrast agents may make MRI a very attractive alternative to the current standard CTA as the imaging technique of choice for regular follow-up of thoracic stent grafts. The rather long acquisition times in this study of about 30 min per patient were well tolerated by the patients.

References

1. Orend KH, Zarbis N, Schelzig H et al (2007) Endovascular treatment (ENT) of acute traumatic lesion of descending thoracic aorta −7 years' experience. Eur J Vasc Endovasc Surg 34:666–672
2. Kouchoukos NT, Bavaria JE, Coselli JS et al (2006) Task force on endovascular surgery; workforce on adult cardiac surgery; council on education and member services; the society of thoracic surgeons. Guidelines for credentialing of practitioners to perform endovascular stent-grafting of the thoracic aorta. J Thorac Cardiovasc Surg 131:530–532
3. Hoornweg LL, Dinkelman MK, Goslings et al (2006) Endovascular management of traumatic ruptures of the thoracic aorta: a retrospective multicenter analysis of 28 cases in The Netherlands. J Vasc Surg 43:1096–1102
4. Rousseau H, Dambrin C, Marcheix B et al (2005) Acute traumatic aortic rupture: a comparison of surgical and stentgraft repair. J Thorac Cardiovasc Surg 129:1050–1055
5. Nico D, Vos PM, de AJM Mol et al (2002) Emergency endovascular treatment of thoracic aortic rupture in three accident victims with multiple injuries. J Endovasc Ther 9 (II):60–66
6. Lobato AC, Quick RC, Philips B et al (2000) Immediate endovascular repair for descending thoracic aortic transection secondary to blunt trauma. J Endovasc Ther 7:16–20
7. Svensson LG, Kouchoukos NT, Miller DC et al (2008) Society of thoracic surgeons endovascular surgery task force: expert consensus document on the treatment of descending thoracic aortic disease using endovascular stent-grafts. Ann Thorac Surg 85:S1–S41
8. Sunder-Plassmann L, Orend KH (2005) Stentgrafting of thoracic aorta complications. J Cardiovasc Surg 121–130
9. Lohan DG, Krishnam M, Saleh R et al (2008) MR imaging of the thoracic aorta. Magn Reson Imaging Clin N Am 16:213–234
10. Arpasi PJ, Bis KG, Shetty AN et al (2000) MR angiography of the thoracic aorta with an electrocardiographically triggered breath-hold contrast-enhanced sequence. Radiographics 20:107–120
11. Amano Y, Takahama K, Kumita S (2008) Non-contrast-enhanced MR angiography of the thoracic aorta using cardiac and navigator-gated magnetization-prepared three-dimensional steady-state free precession. J Magn Reson Imaging 27:504–509
12. François CJ, Tuite D, Deshpande V et al (2008) Unenhanced MR angiography of the thoracic aorta: initial clinical evaluation. Am J Roentgenol 190:902–906
13. Koktzoglou I, Kirpalani A, Carroll TJ et al (2007) Dark-blood MRI of the thoracic aorta with 3D diffusion-prepared steady-state free precession: initial clinical evaluation. Am J Roentgenol 189:966–972
14. van Herwaarden JA, Muhs BE, Vincken KL et al (2006) Aortic compliance following EVAR and the influence of different endografts: determination using dynamic MRA. J Endovasc Ther 13:406–414
15. Pujadas S, Reddy GP, Weber O et al (2006) Phase contrast MR imaging to measure changes in collateral blood flow after stenting of recurrent aortic coarctation: initial experience. J Magn Reson Imaging 24:72–76
16. Hom JJ, Ordovas K, Reddy GP (2008) Velocity-encoded cine MR imaging in aortic coarctation: functional assessment of hemodynamic events. Radiographics 28:407–416
17. Merkle EM, Klein S, Krämer SC, Wisianowsky C (2002) MR angiographic findings in patients with aortic endoprostheses. Am J Roentgenol 178:641–648
18. Klemm T, Duda S, Machann J et al (2000) MR imaging in the presence of vascular stents: a systematic assessment of artifacts for various stent orientations, sequence types, and field strengths. J Magn Reson Imaging 12:606–615
19. Shellock F, Shellock V (1999) Metallic stents: evaluation of MR imaging safety. Am J Roentgenol 173:543–547
20. Engellau L, Olsrud J, Brockstedt S et al (2000) MR evaluation ex vivo and in vivo of a covered stent-graft for abdominal aortic aneurysms: ferromagnetism, heating, artifacts, and velocity mapping. J Magn Reson Imaging 12:112–121
21. Buecker A, Spuentrup E, Ruebben A et al (2002) Artifact-free in-stent lumen visualization by standard magnetic resonance angiography using a new metallic magnetic resonance imaging stent. Circulation 105:1772–1775
22. Hilfiker PR, Quick HH, Schmidt M et al (1999) In vitro image characteristics of an abdominal aortic stent graft: CTA versus 3D MRA. Magma 8:27–32
23. Merkle EM, Klein S, Wisianowsky C et al (2002) Magnetic resonance imaging versus multislice computed tomography of thoracic aortic endografts. J Endovasc Ther 9:II2–II13
24. Weigel S, Tombach B, Maintz D et al (2003) Thoracic aortic stent graft: comparison of contrast-enhanced MR angiography and CT

angiography in the follow-up: initial results. Eur Radiol 13:1628–1634
25. Farhat F, Attia C, Boussel L et al (2007) Endovascular repair of the descending thoracic aorta: mid-term results and evaluation of magnetic resonance angiography. J Thorac Cardiovasc Surg 48:1–6
26. Krämer SC, Wall A, Maintz D et al (2004) 3.0 Tesla magnetic resonance angiography of endovascular aortic stent grafts: phantom measurements in comparison with 1.5 Tesla. Investig Radiol 39:413–417
27. Engellau L, Larsson EM, Albrechtsson U et al (1998) Magnetic resonance imaging and MR angiography of endoluminally treated abdominal aortic aneurysms. Eur J Vasc Endovasc Surg 15:212–219
28. Pieper S, Lorensen B, Schroeder W et al (2006) The NA-MIC Kit: ITK, VTK, Pipelines, Grids and 3D Slicer as an Open Platform for the Medical Image Computing Community. Proceedings of the 3rd IEEE International Symposium on Biomedical Imaging: From Nano to Macro 1:698–701
29. Pieper S, Halle M, Kikinis R (2004) 3D SLICER. Proceedings of the 1st IEEE International Symposium on Biomedical Imaging: From Nano to Macro 1: 632-635
30. Gering D, Nabavi A, Kikinis R et al (1999) An Integrated visualization system for surgical planning and guidance using image fusion and Interventional Imaging. Int Conf Med Image Comput Comput Assist Interv 2:809–819
31. Grobner T (2006) Gadolinium—a specific trigger for the development of nephrogenic fibrosing dermopathy and nephrogenic systemic fibrosis? Nephrol Dial Transplant 21:1104–1108
32. Marckmann P, Skov L, Rossen K et al (2006) Nephrogenic systemic fibrosis: suspected causative role of gadodiamide used for contrast-enhanced magnetic resonance imaging. J Am Soc Nephrol 17:2359–2362
33. Shimada I, Rooney SJ, Farnati PA et al (1999) Reproducibility of thoracic aortic diameter measurement using computed tomographic scans. Eur J Cardiothorac Surg 16:59–62
34. Lu TLC, Rizzo E, Marquez-Vidal PM et al (2010) Variability of ascending aorta diameter measurements as assessed with electrocardiography-gated multidetector computerized tomography and computer assisted diagnosis software. Interact Cardiovasc Thorac Surg 10:217–221